






## Article

# Application of Response Surface Design for Optimization of Direct Red Dye Biosorption onto Cockleshells

Zakaria Laggoun <sup>1</sup>, Amel Khalfaoui <sup>1</sup>, Abderrezzaq Benalia <sup>2,3</sup>, Amira Fadia Ghomrani <sup>2,4</sup>,  
Raouf Bouchareb <sup>2</sup>, Asma Mahfouf <sup>2</sup>, Antonio Pizzi <sup>5</sup>, Antonio Panico <sup>6</sup> and Kerroum Derbal <sup>2,\*</sup>

- <sup>1</sup> Laboratory of Environmental Process Engineering (LIPE), Department of Environmental Engineering, Faculty of Engineering Process, University Salah Boubnider-Constantine 3, New City Ali Mendjeli, Constantine 25000, Algeria; zakaria.laggoun@univ-constantine3.dz (Z.L.); amel.kalfaoui@univ-constantine3.dz (A.K.)
- <sup>2</sup> Laboratory of Process engineering for Sustainable Development and Health Products (GPDDPS), National Polytechnic School of Constantine, Department of Process Engineering, Constantine 25000, Algeria; benalia.abderrezzak@gmail.com (A.B.); a.ghomrani@univ-soukahras.dz (A.F.G.); boucharebraouf@yahoo.fr (R.B.); mahfouf.asma@yahoo.fr (A.M.)
- <sup>3</sup> Higher Normal School of Constantine, New City Ali Mendjeli, Constantine 25000, Algeria
- <sup>4</sup> Physics of Matter and Radiation Laboratory (LPMR), Department of Process Engineering, Faculty of Science and Technology, University Mohamed Cherif Messaadia, BP 1553, Souk Ahras 41000, Algeria
- <sup>5</sup> Laboratoire d'Etude et Recherche sur le Matériau Bois (LERMAB), Ecole Nationale Supérieure des Technologies et Industries du Bois (ENSTIB), University of Lorraine, 27 Rue Philippe Seguin, 88000 Epinal, France; antonio.pizzi@univ-lorraine.fr
- <sup>6</sup> Department of Engineering, University of Campania L. Vanvitelli, 81031 Aversa, Italy; antonio.panico1@unicampania.it
- \* Correspondence: derbal\_kerroum@yahoo.fr; Tel.: +213-697812907

**Abstract:** This work emphasizes the efficiency of the response surface design to optimize the parameters affecting the removal of a textile dye—Direct Red 81 (DR-81)—by biosorption on seafood waste, namely, cockleshells (CS). The adsorbent was characterized by X-ray diffraction (XRD), Fourier-transform infrared spectroscopy (FTIR), energy-dispersive X-ray spectroscopy (EDX), thermogravimetric analysis (TGA), scanning electron microscopy (SEM), and Brunauer–Emmett–Teller (BET) analysis of surface and pH points of zero charge ( $\text{pH}_{\text{pzc}}$ ). A Box–Behnken design (BBD) with three factors was used to optimize the experimental conditions. After the experiment and data analysis, the optimal conditions found were 1 g of adsorbents, 10 mg/L of initial dye concentration, and a pH of 2 in the adsorbate solution, with the highest removal efficiency of 99.98%. The experimental results were analyzed by the ANOVA test, and they demonstrated the acceptability of the quadratic regression model. The adjusted determination coefficient  $R^2$  (adj) was equal to 98.82%, indicating an excellent relationship between the predicted and experimental responses. Langmuir isotherms were determined to be the best-fitting model, and the maximum adsorption capacity was 4.65 mg/g. The adsorption process was endothermic and fit the pseudo-second-order model. The negative values of  $\Delta H$  and  $\Delta S$  in the thermodynamic research showed that the bio-adsorption technique for the removal of Direct Red 81 is exothermic, spontaneous, and feasible. In addition, the negative value of  $\Delta G$  indicates that the adsorption mechanism occurs at solid–liquid interfaces with an increasing number of species.

**Keywords:** cockleshells; bio-adsorption; Direct Red 81; RSM; Box–Behnken



**Citation:** Laggoun, Z.; Khalfaoui, A.; Benalia, A.; Ghomrani, A.F.; Bouchareb, R.; Mahfouf, A.; Pizzi, A.; Panico, A.; Derbal, K. Application of Response Surface Design for Optimization of Direct Red Dye Biosorption onto Cockleshells. *Appl. Sci.* **2023**, *13*, 12333. <https://doi.org/10.3390/app132212333>

Academic Editor: Giacomo Dacarro

Received: 12 August 2023

Revised: 5 September 2023

Accepted: 9 September 2023

Published: 15 November 2023



**Copyright:** © 2023 by the authors. Licensee MDPI, Basel, Switzerland. This article is an open access article distributed under the terms and conditions of the Creative Commons Attribution (CC BY) license (<https://creativecommons.org/licenses/by/4.0/>).

## 1. Introduction

Water pollution is a phenomenon that has a negative impact on both human health and ecosystems [1]. The most polluting dyes allowed are mainly used in the leather, plastic, mineral oil, and cosmetic wax industries [2], as well as in other industries such as food, paper, textiles, and pharmaceuticals, with an annual output of  $7 \times 10^5$  tons [3]. These

dyes are harmful, carcinogenic, mutagenic, toxic, and harmful to human health, and they undoubtedly harm the environment [4].

In previous years, there have been several works on the removal of dyes by biological and physicochemical treatments, including coagulation, flocculation, filtration, advanced oxidation, ion exchange, membrane processes, aerobic and anaerobic degradation [5], membrane distillation [6], electrochemical methods [7], irradiation [8], Fenton reaction [9], reverse osmosis, precipitation, ozonation [1], and adsorption [10]. These treatments are effective yet highly costly, limited in efficiency, and deficient in process selectivity [11]. In addition, other hazardous byproducts are formed and require further treatment, with consequent energy consumption [12].

Compared to other water treatment processes, adsorption is one of the simplest, safest, and most versatile techniques to retain the pollutants [13]. It is the most efficient technique, with minimal use of chemicals, and it is easier to implement in wastewater treatment plants [14].

Bio-adsorption is an approach that is generally applied to eliminate heavy metals [15] and different types of organic pollutants [16]. The use of various alternative adsorbents can be both effective and less expensive in removing organic pollutants, such as nutrients and dyes, according to research [17]. For example: rice husk [18], orange and banana peels [19], bark, pineapple stem waste, water hyacinth pulp powder, tuberous pulp, sugarcane pulp, coconut pulp [20], tea waste, com cob, wheat bran, peanut skin, bamboo activated carbon, modified corncobs, modified cassava waste, lemon peel, durian peel [21], pomelo peel [22], potato peel [23], chitosan, zeolite, and activated carbon [24].

Cockleshells have become a major source of protein in Southeast Asia and a source of calcium carbonate ( $\text{CaCO}_3$ ) in Malaysia. The strong demand for marron-based seafood has generated a considerable quantity of shellfish. A number of studies have been conducted to utilize waste cockleshells as valuable materials. For example, the mineral content of  $\text{CaCO}_3$  in shell waste can be converted into lime to be used as a heterogeneous catalyst in biodiesel production, biolubricant production, and also as an adsorbent in wastewater treatment processes [25].

Cockleshells may be considered to be an inexpensive source of  $\text{CaCO}_3$ . They are composed of  $\text{CaCO}_3$ , mainly as a mineral calcite or aragonite.  $\text{CaCO}_3$  is gaining a lot of attention for its role as a heavy metal adsorbent.  $\text{CaCO}_3$  is a must for adsorbents because it can be regenerated with low-cost HCl to desorb heavy ions and maintain high adsorption capacities after multiple cycles. Using cockleshells as an adsorbent could represent an economic and environmental way forward, as the process is highly efficient and uses low-cost materials for the exploitation of aquaculture waste products to achieve a zero-waste production system [26].

Cockleshells, which are natural marine waste, were used as bio-adsorbents in this research.

The cockleshells were evaluated for removing Direct Red 81 from aqueous solutions.

The effects of time, initial concentration, mass of bio-adsorbent, temperature, and solution pH were studied to find the optima of these effects on the adsorption of DR-81. Kinetics, thermodynamics, and optimization by Box–Behnken design were studied.

## 2. Materials and Methods

### 2.1. DR-81 Solution

Direct Red 81 is a toxic, sulfonated, azo-based anionic dye. The structure is given in Figure 1; molar mass: 676 g/mol; chemical structure:  $\text{C}_{29}\text{H}_{19}\text{N}_5\text{N}_2\text{O}_8\text{S}_2$ ; wavelength: 509.8 nm, was procured from Sigma Aldrich (St. Louis, MO, USA). First, the stock solution (1 g/L) was prepared by dissolving 1 g of Direct Red 81 in a volume of 1000 mL of distilled water. The pH of the solution was adjusted by adding concentrations of (0.1–1 N) HCl or (0.1–1 N) NaOH.

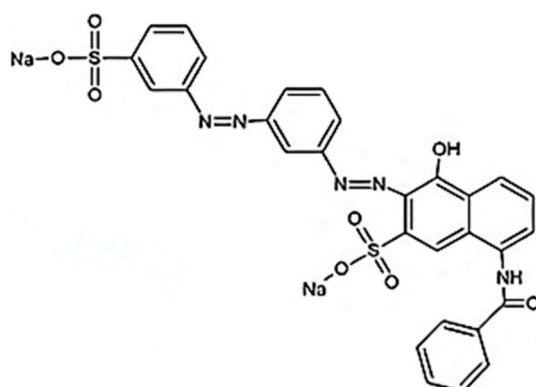


**Figure 1.** Structure of DR-81 [27].

## 2.2. Preparation of the Adsorbent

Cockleshells were collected from the beach of Djenah in the region of Jijel, Algeria. They were prepared by the following steps: washed several times with distilled water to eliminate the impurities, smoothed to dry in ambient air, and then crushed and sieved to obtain granules of diameter  $d \leq 125 \mu\text{m}$ . Later, they were stored in a desiccator.

## 2.3. Adsorption Experiments

The batch adsorption study was carried out to determine the optimal operating conditions for the following effects: dose of bio-adsorbent (0.3–1.5 g); initial dye concentration (10–100 mg/L); contact time (0–60 min); and temperature (22–31–61 °C), and the pH of the solution (2–12) was adjusted by adding concentrations of (0.1–1 N) HCl or (0.1–1 N) NaOH. Adsorption kinetics were determined by contacting a 100 mL volume of Direct Red dye 81 at a concentration of 10 mg/L with a mass of 0.5 g of bio-adsorbent in ambient air, with a stirring speed of 300 rpm in a 60 min contact time. The samples were filtered by centrifugation (HETTICH ROTOFIX 32A, Andreas Hettich, Tuttlingen, Germany) at 4000 rpm in an 8 min rotation time. The supernatants were analyzed by UV–visible spectroscopy (JASCO V-750) at a wavelength of 509.8 nm.

The adsorption capacity ( $q_e$ ) and the percentage of dye removal were calculated using the following equations [27]:

$$q_e = \frac{(C_0 - C_e) * V}{m} \quad (1)$$

$$R(\%) = \left( \frac{C_0 - C_t}{C_0} \right) * 100 \quad (2)$$

where  $C_0$  and  $C_e$  are the initial dye concentration (mg/L) and the equilibrium dye concentration (mg/L), respectively,  $V$  is the volume of the solution (L), and  $m$  is the mass of the adsorbent.

## 2.4. Characterization of Cockleshell Powder

In order to identify the behavior of the biomaterial used in this study, a number of analyses were applied. Thermogravimetric analysis (TGA) and differential scanning calorimetry (DSC) were carried out using a METTLER TOLEDO thermal analyzer in the range of 30–906 °C, with a heating rate of 30 °C/min (METTLER TOLEDO GmbH, Gießen, Germany). FTIR (CHIMADZU Code: HI 98713, Chimadzu, Cluj-Napoca, Romania) was used to find the IR spectra of the CS adsorbent in the range of 400–4500  $\text{cm}^{-1}$ , using a JASCO FT/IR 4600. X-ray diffraction (XRD: D8-Discover) analysis was performed using an X-ray diffractometer of the PHASER-BRUKER brand in the range of 20–80°. SEM was used to provide information on shell morphology. The aim of using EDX (BRUKER X/6/10, Billerica, MA, USA) was to determine the composition of the present elements in the sample using a THERMO FISHER QUATTROS (Thermo Fisher Scientific, Waltham,

MA, USA). Finally, the BET (Quantachrome Instruments Corporate Headquarters, Boynton Beach, FL, USA) analysis to determine the area of the biosorbent was carried out using a Quantachrome® ASiQwin instrument version 5.21.

The purpose of the characterization of the biosorbent by the  $pH_{pzc}$  value was to find the degree and charge of ionization on the surface of the biosorbent at different solution pH values. The protocol of  $pH_{pzc}$  was as follows: the homogenization of a mass of biosorbent (0.15 g) with a volume (50 mL) of NaCl solution (0.01 M) at different pH values (2–12). The NaCl samples were adjusted with NaOH (0.01 N) and HCL (0.01 N) solutions, and the  $pH_F$  values were measured after stirring for 48 h at room temperature. The intersection of  $[(pH_F - pH_i) \text{ vs. } (pH_i)]$  gives the  $pH_{pzc}$  value [28].

### 2.5. Experimental Design

The optimization of the removal of Direct Red dye 81 by bio-adsorption was carried out by the surface response methodology (RSM). The Box–Behnken design (BBD) is particularly noteworthy.

The main objective of this method is to optimize various processes, and it is commonly used for experimental design [14]. The method’s aim (RSM) is to enhance the surface response optimization, which is influenced by different parameters that are identified by a mathematical model of the surface response as a function of individual interaction and quadratic effects.

In this part, the effects of the following parameters were examined: concentration (mg/L), mass of bio-adsorbent (g), and pH of the aqueous solution. Table 1 shows the actual and coded values of the studied effects.

**Table 1.** Experimental ranges and levels of the factors studied in the Box–Behnken design.

Variable	Symbol	Levels of Coded Variables		
		Low	Medium	High
Concentration (mg/L)	X1	−1	0	+1
Biosorbent dose (g)	X2	10	55	100
pH	X3	0.3	0.9	1.5
		2	7	12

The relationship between the Y response and the independent variables can be presented by the following quadratic model [29]:

$$Y(R\%) = b_0 + \sum b_i X_i + \sum b_{ij} X_{ij} + \sum b_{ii} X_i^2 \tag{3}$$

where  $b_0$  is the model constant;  $b_i$ ,  $b_{ij}$ , and  $b_{ii}$  are the regression coefficients;  $X_i$  represents the individual effects;  $X_{ij}$  represents the interaction effects; and  $X_{ii}$  represents the quadratic effects.

## 3. Results and Discussion

### 3.1. Characterization of Cockleshell Powder

#### 3.1.1. Point of Zero Charge

According to Figure 2, it is the lower pH value of  $pH_{pzc}$  on the passively charged biosorbent surface that favors the formation of attractive forces with the anionic dye (DR-81). Conversely, when the pH exceeds the  $pH_{pzc}$  value, the biosorbent surface is negatively charged, forming repulsive forces with the anionic dye [30].

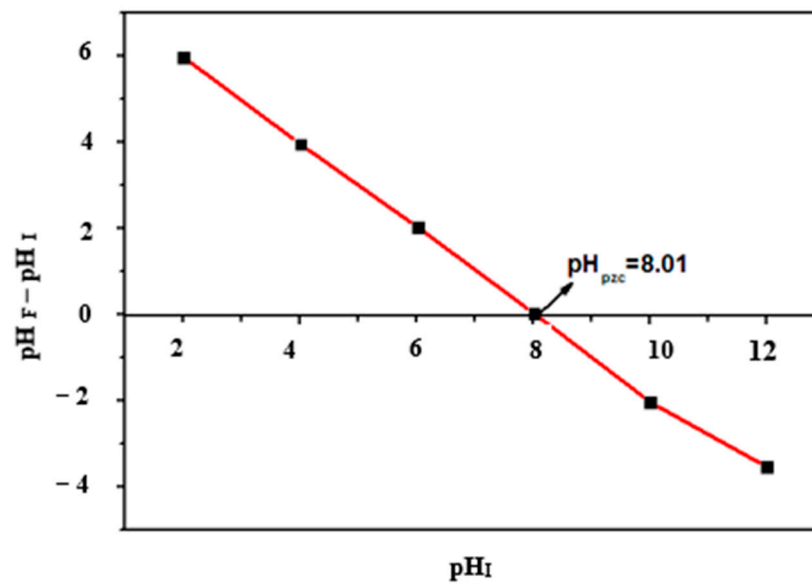


**Figure 2.** The curve of  $\Delta\text{pH}$  vs.  $\text{pH}_i$  for determination of the  $\text{pH}_{\text{pzc}}$  of CS powder.

### 3.1.2. Thermogravimetric Analysis (TGA) and DSC

The main purpose of TGA and DSC analysis is to characterize materials by studying the variation in material mass as a function of time or temperature and the heat exchange between a sample and a reference. Figure 3 shows the TGA and DSC graphs.

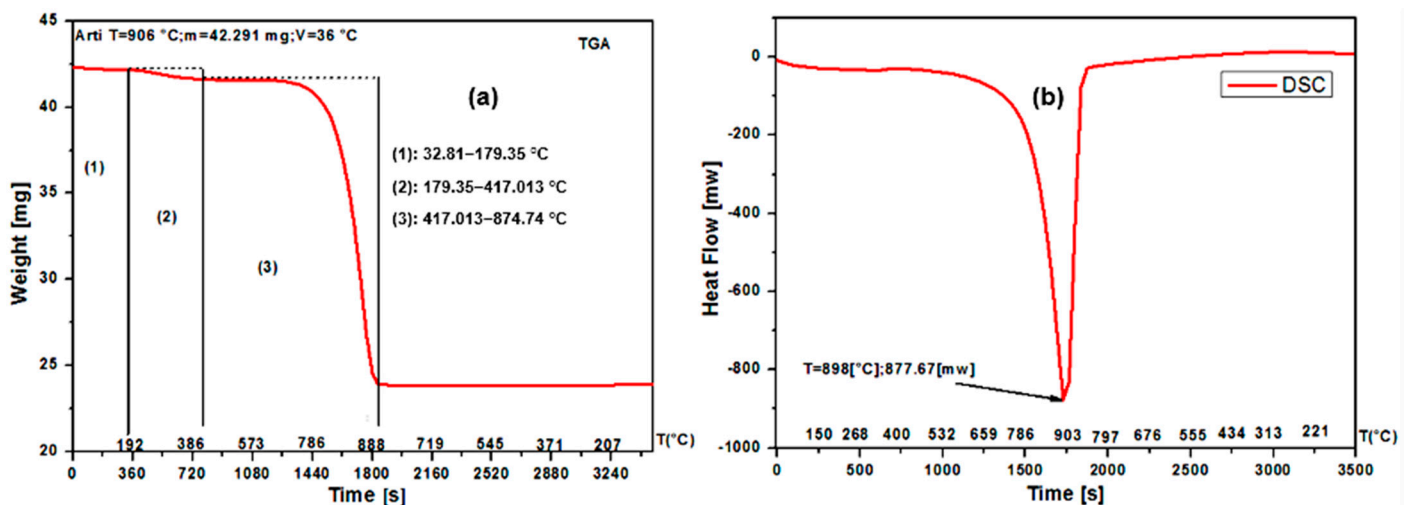


**Figure 3.** The graphs: (a) thermogravimetric analysis (TGA) and (b) differential scanning calorimetry (DSC) of cockleshell powder.

From Figure 3a, we can note the presence of three stages of mass loss: The first loss of 0.25% mass can be attributed to the evaporation of moisture present in the cockleshell powder [26]. The second loss (1.55%) is due to the dehydration of the water in the carbonate network due to the transformation of the aragonite phase (unstable phase) towards the calcite phase [31]. The third loss is a stage of rapid degradation of the mass up to a percentage of 43.51%, which represents the decomposition of calcium carbonate and the formation of calcium oxide with the release of carbon dioxide—a reaction that has already been recorded [32].

A stabilization phase can also be observed: the weight of the sample remains almost stable from temperatures above 874.76 °C, indicating the complete formation of calcium oxide [26] with purity of 43.51%.

The DSC graph in Figure 3b shows a single endothermic peak at 898 °C, which represents the melting temperature of the material. The presence of a single peak shows that the cockleshell powder contains a single phase, giving an idea of the purity of the sample.

### 3.1.3. FTIR Analysis

According to the existing literature, carbonate groups play a greater role in determining the bonds between the surface of the CS adsorbent and Direct Red 81 dye (DR-81). There are four vibration modes assigned: asymmetric stretching mode (V1), out-of-plane bending (V2), doubly degenerate planar symmetry (V3), and doubly degenerate planar bending mode (V4) [33].

Figure 4 shows the appearance of the micrometric bands of raw cockleshell powder, with peaks at 711.6, 855.27, 1080.91, 1449.24, and 1786.72  $\text{cm}^{-1}$ . After the adsorption of the DR-81 dye, a slight transition in the position of certain peaks was observed, but no change in structure was observed due to the appearance or disappearance of other peaks. This may be attributed to the conservation of the physicochemical properties [34] of the CS adsorbent after the adsorption of DR-81.

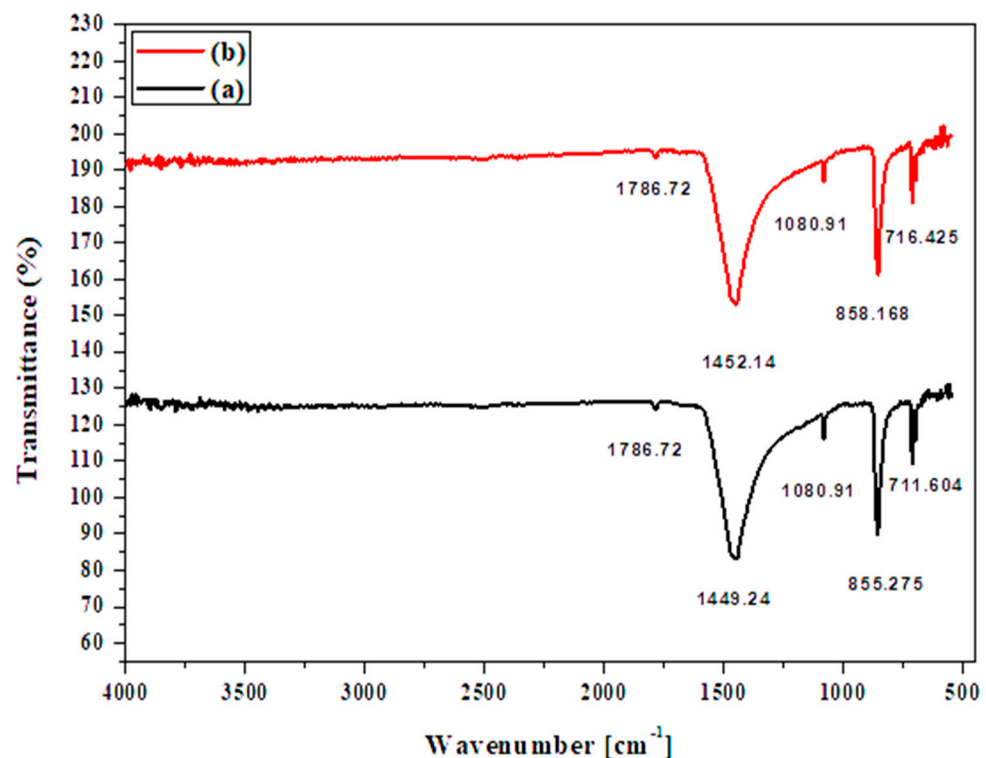


**Figure 4.** FTIR spectrum of cockleshell (CS) powder (a) before and (b) after DR-81 adsorption.

The presence of the 711.6  $\text{cm}^{-1}$  band indicates that there is a structural change in the calcium ions with respect to the symmetry of the calcite phase (V4), which also represents the band of the aragonite phase [33]. The appearance of the peaks at 855.27 and 1080.91  $\text{cm}^{-1}$  represents the inactive carbonate ions ( $\text{CO}_3^{2-}$ ) of the aragonite phase [35] assigned by the vibration modes V2 and V1, respectively. The appearance of a large peak at 1449.24  $\text{cm}^{-1}$  can also be explained by the structural change in the symmetry of the aragonite phase assigned to vibration mode V3, or by the presence of alkyl groups in the polymorphic aragonite phase [31].

Finally, the peak at 1786.72  $\text{cm}^{-1}$  is clear evidence of the presence of a single crystalline domain of the aragonite phase. Additionally, it confirms the fundamental changes in the vibrational mode positions of the sample resulting from the modification of the electrostatic valence of the CaO bond due to changes in the oxygen atoms in the environment [31].

### 3.1.4. X-ray Diffraction Analysis (XRD)

The use of XRD gives information on the molecular structure and morphological shape of the cockleshells. Figure 5 shows the XRD of cockleshell powder before and after the adsorption of the Direct Red 81 dye.

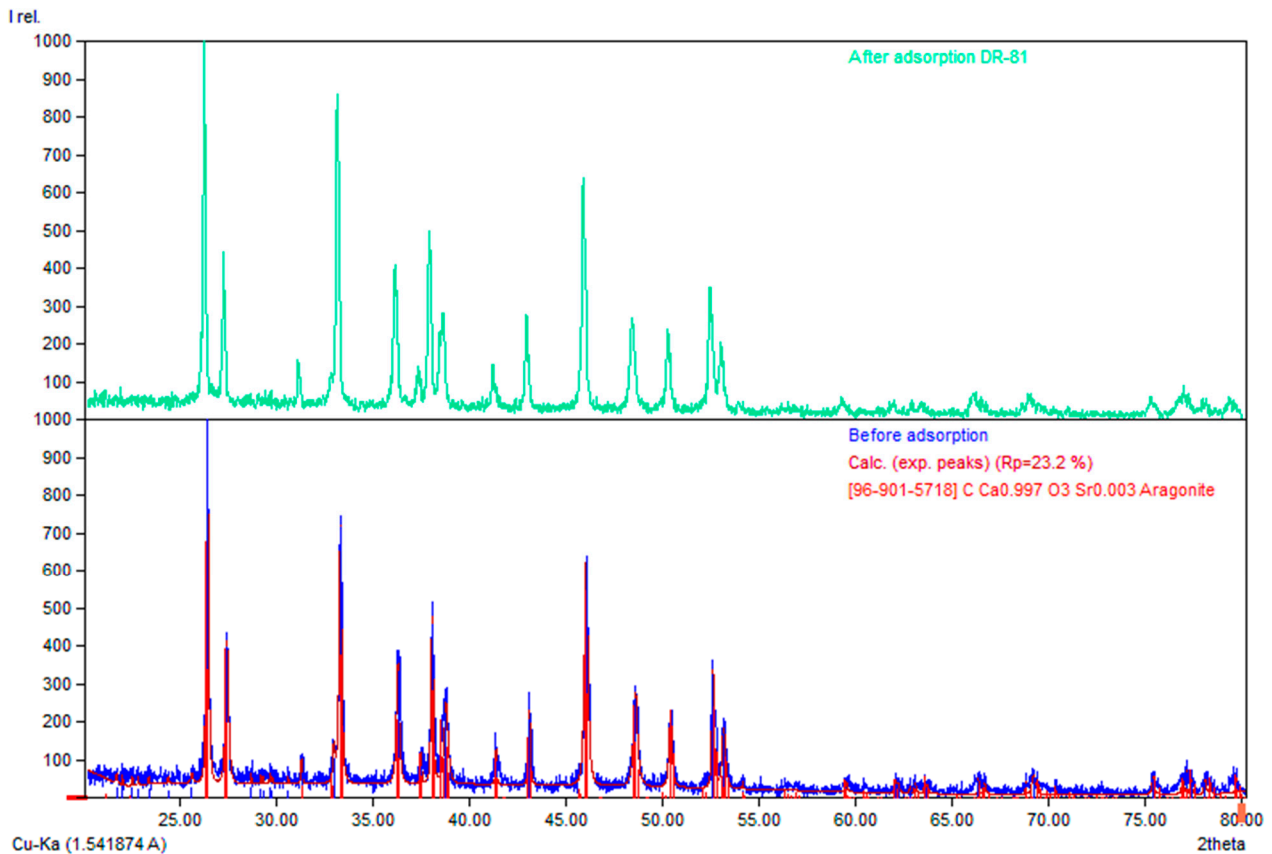


**Figure 5.** XRD of cockleshell powder before and after adsorption of DR-81.

Figure 5 shows the presence of  $\text{CaCO}_3$  (aragonite) at positions 2 theta of 26.03, 27.25, 33.07, 36.11, 38.54, 41.09, 42.90, 45.82, 48.37, 52.38, and 53. These two positions correspond to the crystal planes (1 1 1), (0 2 1), (0 1 2), (1 0 2), (1 1 2), (0 2 2), (1 3 1), (2 2 0), (2 2 1), (0 4 1), (1 3 2), (1 1 3), and (0 2 3), respectively. Other parameters include  $a = 4.95410 \text{ \AA}$ ,  $b = 7.94940 \text{ \AA}$ , and  $c = 5.71860$ , with an orthorhombic crystal system.

The assignments of position 2 and other parameters for aragonite from XRD were in agreement with the reference code [96-901-5718] of a hexagonal crystal system, with the characteristic peak positioned at 2 theta = 26.03 and the crystal plane of (1 1 1). A similar study was conducted by [32].

There was also no change in the cockleshell powder's peaks after the adsorption of DR-81. This latter observation indicates that the adsorption of DR-81 dye does not change the physicochemical properties [34] of the CS adsorbent.

### 3.1.5. Scanning Electron Microscopy (SEM) and BET Analysis

Nitrogen adsorption–desorption isotherms were used to determine the textural parameters of porous materials using the Brunauer–Emmett–Teller method. The specific surface area of CS was  $50.954 \text{ m}^2/\text{g}$ , with a pore volume equal to  $0.893 \text{ mL/g}$  and a pore radius of  $151.536 \text{ \AA}$ .

Based on the IUPAC classification of adsorption isotherms, the BET revealed the following:

The  $\text{N}_2$  isotherm resembled type III, with a high adsorption capacity, while indicating the presence of larger pore-size distributions, narrower mesopores, and larger micropores.

The small hysteresis in the N<sub>2</sub> adsorption–desorption isotherm indicates the capillary condensation phenomenon, which indicates a mesoporous nature [36].

From Figure 6a, it can be observed that the shells present an irregular and non-uniform shape. Therefore, according to the literature, the shells have a needle [37,38] and plate structure with parallel cleavages [26].

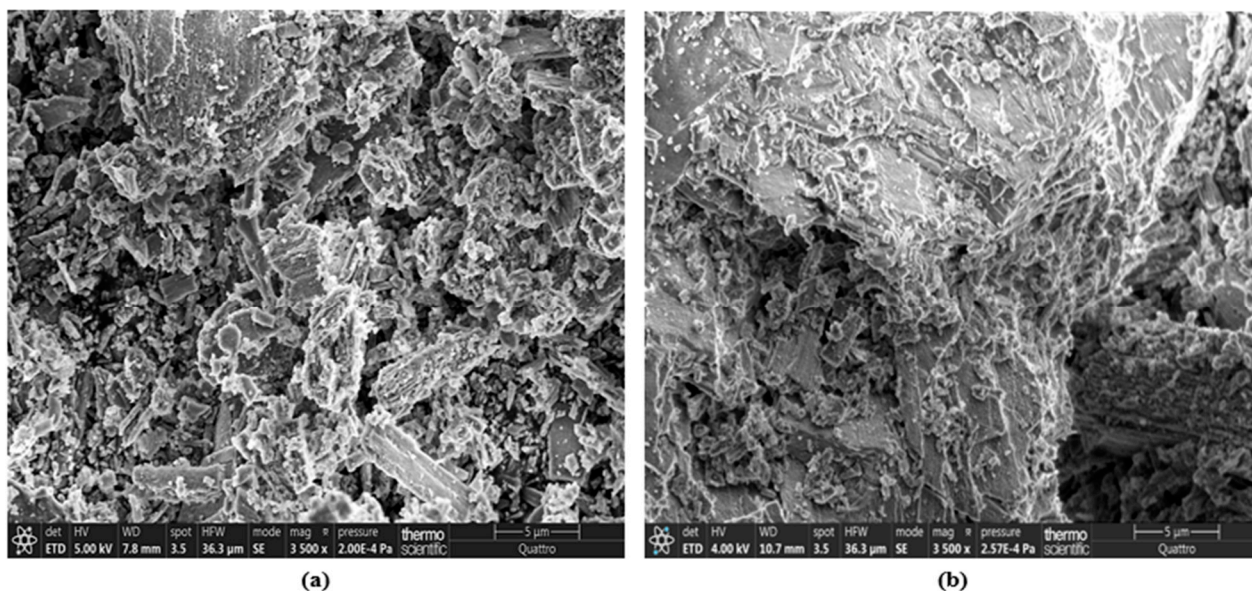


**Figure 6.** SEM of CS (a) before adsorption and (b) after adsorption of DR-81.

From Figure 6b, it can be observed that the initially empty sites of CS become full; this can be explained by an agglomeration of DR 81 molecules after adsorption onto the solid surface of CS.

Aronson and Machlis used both alkaline digestion methods and sonic oscillation to isolate the hyphal walls of *Allomyces macrogynus* [39]. Both types of preparation showed the walls to consist of chitin, glucan, and ash. In addition, the mechanically isolated walls contained a protein fraction whose properties and the significance thereof were not determined. Hemicellulose-type polysaccharides, pectic substances, ether-soluble lipids, and constituents gave rise to 3-*O*- $\alpha$ -carboxyethyl hexosamine that was not found in the walls. The walls of plants grown for 60–70 h under the prescribed conditions contained approximately 60% chitin, 15% glucan, 10% ash, and 10% protein intimately associated with the walls. The percentage of wall material in a mycelium, as well as the percentage of chitin in the walls, increases with the chronological age of the mycelium. These percentages are not, however, affected by variations in the composition of the nutrient medium. The chitin in the walls could be hydrolyzed in the presence of chitinase or lysozyme, yet it had no detectable effect on the walls.

### 3.1.6. Elemental Composition of Cockleshells

The chemical composition of the cockleshell powder samples was analyzed using EDX.

Figure 7a shows that the shell powder sample presented the following chemical composition: oxygen, carbon, calcium, and traces of strontium (Sr). The chemicals' percentages are illustrated in the table within the figure, and they formed a salt phase of CaCO<sub>3</sub> in aragonite form, which is consistent with the results of the FTIR and XRD.



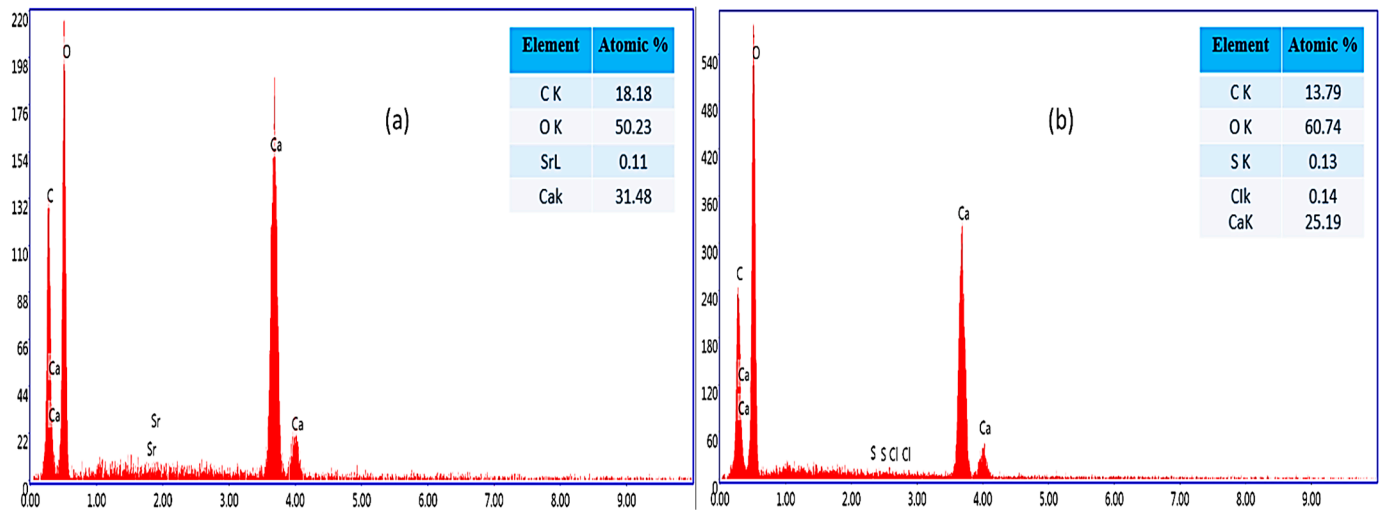


Figure 7. EDX of cockleshell powder (a) before and (b) after adsorption of DR-81.

After the adsorption of DR-81, an agglomeration of the dye molecules presented by the chemical compositions of sulfur and chlorine at a low trace percentages is illustrated in Figure 7b.

### 3.2. Parameter Study of the Adsorption of DR-81 onto the Cockleshell Powder

#### 3.2.1. Effect of Adsorbent Dose

It is important to know the mass transfer phenomenon of DR-81 removal by the CS, in the range of 0.3–1.5 g. Figure 8 depicts the effect of biosorbent dosage on the DR-81 removal efficiency and adsorption capacity.

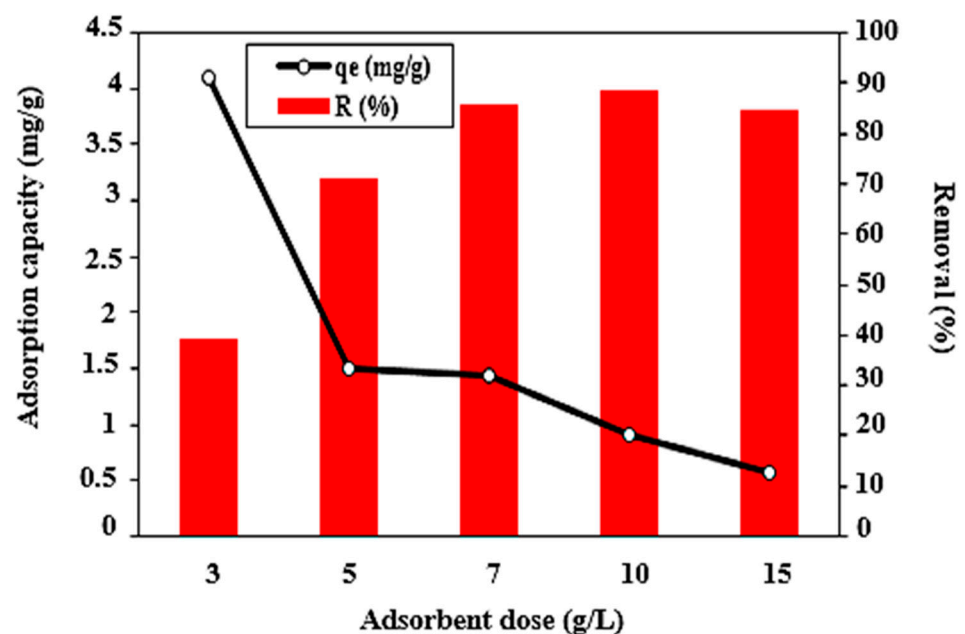


Figure 8. Effect of CS dosage on removal efficiency and adsorption capacity for DR-81 ( $C_0 = 10$  mg/L,  $V = 100$  mL,  $T = 22$  °C,  $pH = 7.09$ , stirring speed = 300 rpm).

According to Figure 8, the removal efficiency data present two stages: In the first stage, in the adsorbent dose range of 0.3–1 g/L, there is an increase in removal efficiency from 39 to 88.06%. This phenomenon could be attributed to the presence of a large number of unsaturated active sites [40]. The second stage marks an increase in the CS dosage in the range 1–1.5 g/L, with a decrease in removal efficiency from 88.06% to 84.73%. In

this stage, the vacant sites of CS are totally charged by dye. Simultaneously, the capacity of adsorption of DR-81 by CS decreases from 4.52 to 1.20 mg/g with the increase in the biosorbent dosage from 0.3 to 1.5 g/L. This result could be explained mathematically in the expression of the adsorption capacity ( $q_e$ ) cited in Equation (1). When the biosorbent dose rises,  $q_e$  automatically decreases.

### 3.2.2. Effects of Initial Dye Concentration and Contact Time

The effects of the initial concentration and contact time are the two main factors to determine the maximum adsorption capacity for DR-81 dye removal by cockleshells in the interval 0–60 min, and to control the adsorption mechanisms at different concentrations from 10 to 100 mg/L. The effects of the initial dye concentration and contact time on DR-81 removal are presented in Figure 9.

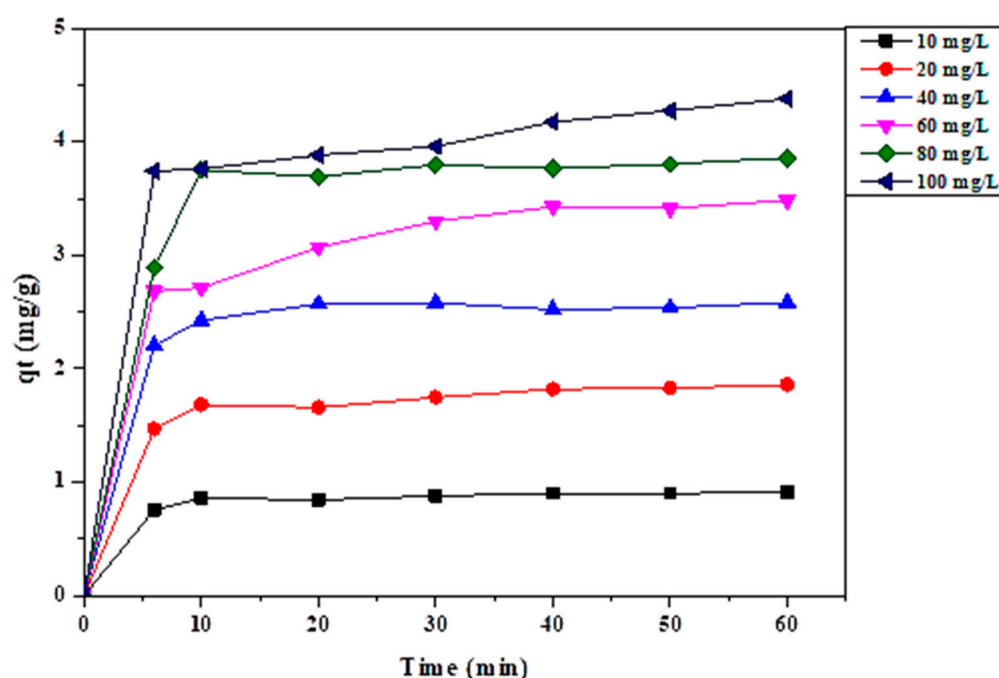


**Figure 9.** Effects of initial concentration and contact time on DR-81 removal efficiency ( $C_0 = 10$  mg/L,  $m = 0.5$  g,  $pH = 7.09$ ,  $T = 22$  °C,  $v = 300$  rpm).

According to Figure 9, the first part of the curves (0–10 min) describes the rapid evolution of the adsorption capacity and is explained by the great availability of active sites on the solid surface. The second part of the curves (10–60 min) is a slow increase in and stabilization of the percentage of elimination, which indicates that the DR-81 molecules are in a phase of progressively occupying the available active sites and causing the saturation of the bio-adsorbent surface [41]. The increase in the concentration from 10 to 100 mg/L with an increase in the adsorption capacity from 1.47 to 6.79 mg/L is also explained by the decreasing attraction forces between the DR-81 dye and the solid surface [40].

### 3.2.3. Effect of the Temperature

The effect of temperature is of paramount importance; since it affects the adsorption capacity and the percentage of removal of the DR-81 dye in the bio-adsorption process. The adsorption of DR-81 in an aqueous solution was studied in the range of 22 °C to 61 °C. The effect of temperature on the adsorption process is presented in Figure 10.

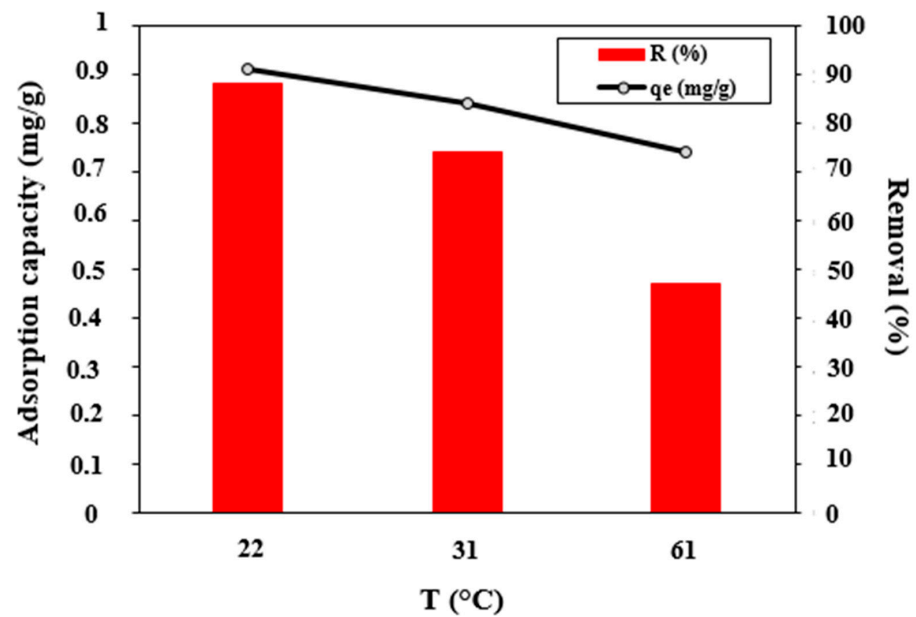


**Figure 10.** Effects of temperature on the removal efficiency and adsorption capacity for DR-81 ( $C_0 = 10$  mg/L,  $m = 1$  g,  $\text{pH} = 7.09$ ,  $v = 300$  rpm).

From the data in Figure 10, the decrease in the removal efficiency of DR-81 from 88 to 67%, and in the capacity of adsorption from 0.88 to 0.74 mg/g, with a rising temperature in the range 22–61 °C, can be explained by weaker adsorption forces between the bio-adsorbent and the DR-81 molecules. This implies that when the temperature increases, either the active sites on the bio-adsorbent surface are damaged [42] or the Brownian movement of the DR-81 molecules increases as the temperature rises.

### 3.2.4. Effect of the pH of the Solution

The effect of pH is crucial in influencing the surface charge of the bio-adsorbent in the solution of DR-81 dye. It was studied in the pH range of 2 to 12. Figure 11 illustrates the impact of pH on the adsorption process of DR-81 dye.

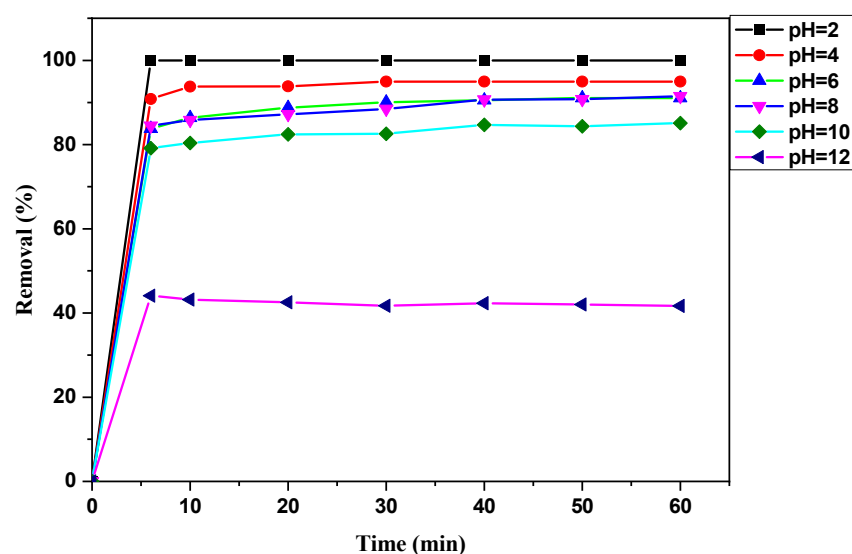


**Figure 11.** Effects of pH solution on the removal efficiency and adsorption capacity for DR-81 ( $C_0 = 10$  mg/L,  $m = 1$  g,  $V = 100$  mL,  $T = 22$  °C, stirring speed = 300 rpm).

The effects of solution pH on the removal of DR-81 are shown in Figure 11. The results indicate that the removal efficiency of the DR-81 dye by CS decreased from 100 to 46% with a large increase in the pH range (2–12). This was responsible for the force of attraction between the solid surface and the functional groups of DR-81. However, when the pH was alkaline ( $\text{pH} > \text{pH}_{\text{PZC}}$ ), the negatively charged bio-adsorbent surface caused the formation of repulsive forces between the bio-adsorbent and DR-81.

These results show that there is a good removal of the Direct Red 81 dye in a very acidic environment ( $\text{pH} = 2$ ). However, since almost all water's pH varies from 6 to 8, a pH of 6 was chosen to give an idea of the adsorption capacity under normal conditions [12].

### 3.3. Adsorption Kinetics and Isotherm

#### 3.3.1. Adsorption Kinetics

The main objective of the kinetic study of the removal of organic pollutants is to know the control mechanisms of the adsorption process as well as the mass transfer and chemical reactions. In this research on the removal of Direct Red 81 textile dye by CS, the following kinetic models were examined: pseudo-first-order, pseudo-second-order, and interparticle diffusion.

The pseudo-first-order (PFO) model was based on the sorption capacity of dye on the particle surface. The form was as follows [43]:

$$\frac{dq}{dt} = k_1(q_e - q_t) \quad (4)$$

After integration using the initial conditions at  $t = 0, q = 0$ , we can obtain the following expression [44]:

$$\ln(q_e - q_t) = -K_1 t + \ln q_e \quad (5)$$

where  $K_1$  represents the pseudo-first-order adsorption rate ( $t^{-1}$ ),  $q_e$  represents the adsorption capacity at equilibrium (mg/g), and  $q_t$  represents the adsorption capacity at time  $t$  (mg/g).

The pseudo-second-order (PSO) model was proposed by Ho and Mackay. This model implies that the adsorption process between the surface of the bio-adsorbent and the pollutant is of the chemical adsorption type. The expression is as follows [45]:

$$\frac{dq}{dt} = k_2(q_e - q_t) \quad (6)$$

After integration using the initial conditions  $t = 0, q = 0$ , and at  $t, q = q_t$ , we obtained the following expression [24]:

$$\frac{1}{q_t} = \frac{1}{K_2 q_e^2} + \frac{1}{q_e} t \quad (7)$$

where  $K_2$  is the pseudo-second-order adsorption constant (mg/g.min).

The intraparticle diffusion model (IPD) allows the diffusion mechanisms of the aqueous phase to be met in the internal pores of the adsorbent, since it is a slow process. The expression below represents the linear form of the model [46]:

$$q_t = K_{\text{int}} t^{1/2} + C \quad (8)$$

where  $K_{\text{int}}$  is the inter-articular diffusion constant (mg/g.min<sup>1/2</sup>), and  $C$  is the thickness of the thin layer (mg/g).

The parameters of the PFO, PSO, and IPD kinetic models for the adsorption of DR-81 onto cockleshells are presented in Table 2.

**Table 2.** Parameters of kinetic models: PFO, PSO, and IPD.

[DR-81] <sub>0</sub> (mg/L)	PFO				PSO			IPD		
	q <sub>e</sub> exp (mg/g)	q <sub>e</sub> cal (mg/g)	K <sub>1</sub> (min <sup>-1</sup> )	R <sup>2</sup>	q <sub>e</sub> cal (mg/g)	K <sub>2</sub> (g/mg·min)	R <sup>2</sup>	K <sub>Id</sub>	C (mg/g)	R <sup>2</sup>
10	0.91	0.174	0.067	0.875	0.92	1.18	0.9994	0.024	0.739	0.750
20	1.86	0.471	0.057	0.917	1.89	0.28	0.9988	0.063	1.391	0.853
40	2.58	0.128	0.034	0.168	2.57	0.15	0.9993	0.053	2.214	0.587
60	3.49	1.303	0.065	0.936	3.62	0.08	0.9988	0.167	2.279	0.942
80	3.8	0.429	0.045	0.548	3.90	0.07	0.9989	0.134	2.927	0.620
100	4.38	0.799	0.040	0.909	4.36	0.05	0.9978	0.125	3.37	0.953

The results of the adsorption kinetics of DR-81 by CS for the PFO, PSO, and DIP models are shown in Table 2. The linear models give the correlation coefficients of the kinetic model PSO ( $R^2 \geq 0.9999$ ), which are better compared to those of the PFO model ( $R^2 \leq 0.936$ ) and the IPD model ( $R^2 \leq 0.942$ ). In addition, the theoretical adsorbed amounts in the PSO model are closer to the experimentally adsorbed amount compared to the other kinetic models. This equality indicates that the adsorption of DR-81 by CS occurs via chemisorption [24] and via electron exchange between the dye and the bio-adsorbent surface through covalent forces [46].

### 3.3.2. Adsorption Isotherm

The model of Langmuir suggests that adsorbate molecules are retained on the solid surface of the biomaterial in a homogeneous state, resulting in the formation of a single layer (monolayer). The model formula is as follows [42]:

$$q_e = \frac{q_{\max} K_L C_e}{1 + K_L C_e} \quad (9)$$

The linear form of Equation (9) gives the following equation [47]:

$$\frac{C_e}{q_e} = \frac{1}{q_{\max}} C_e + \frac{1}{K_L q_{\max}} \quad (10)$$

where  $q_e$  is the adsorption capacity of DR-81 at equilibrium (mg/g),  $q_{\max}$  is the theoretical maximum adsorption capacity of DR-81 (mg/g), and  $C_e$  is the concentration of DR-81 at equilibrium (mg/L). The values of  $q_{\max}$ ,  $K_L$ ,  $R_L$ , and  $R^2$  are presented in Table 3.

**Table 3.** Comparison of the isotherm parameters for the biosorption of DR-81 onto cockleshells.

Adsorption Model	Isotherm Parameters	R <sup>2</sup>
Langmuir	q <sub>max</sub> Cal = 4.65 mg/g K <sub>L</sub> (L/mg) = 0.146 R <sub>L</sub> = [0.406–0.064]	0.982
Freundlich	K <sub>f</sub> = 1.027 mg/g 1/n = 0.364	0.941
Tamkin	B <sub>T</sub> = 0.364 j/mol A <sub>T</sub> = 9.358 L/g b <sub>T</sub> = 6734.752 mg/L	0.97

According to the results in Table 3, there is a convergence between the experimental adsorption capacity and the theoretical adsorption rate calculated by the Langmuir linear equation, with the correlation coefficient  $R^2 = 0.982$ , in contrast to the Freundlich ( $R^2 = 0.941$ ) and Tamkin ( $R^2 = 0.97$ ) models. The Langmuir model is the best model to represent the process of biosorption of DR-81 by cockleshells.

In addition to the fact that the Langmuir model is the representative model of adsorption, another analysis to validate the model can be conducted using the separation factor represented by the following relation [48]:

$$R_L = \frac{1}{1 + K_L C_0} \quad (11)$$

The value of  $R_L$  is between 0 and 1.  $R_L$  decreased gradually with the increase in concentration, showing that the latter favors the adsorption of DR-81 [49].

The results show that CS is effective in treating industrial textile wastewater and removing cationic and anionic dyes, as well as DR-81. Other criteria for the selection of this bio-adsorbent over other bio-adsorbents are durability, recyclability, and low cost. CS can be considered as a potential candidate for use in the removal of dyes present in liquid industrial textile effluents. Table 4 compares the adsorption capacities for a few biomaterials (modified and unmodified) with the CS used in this study.

**Table 4.** Comparison of the maximum biosorption capacity of DR-81 dye onto various adsorbents.

Adsorbent	Adsorption Capacity (mg/g)	References
Soy meal hull	120.5	[50]
Bamboo sawdust	6.43	[51]
Modified bamboo sawdust	13.83	[51]
Chamomile plant	10.1	[52]
Pumice	22.422	[50]
Potato peel	58.8	[53]
Neem bark	10.41	[53]
Activated potato peel	8.4	[53]
Activated neem bark	5.71	[53]
Modified silk maze	30.30	[54]
Soil containing copper	26.2	[40]
Iron filings	25.3	[55]
GO-MVK-ANI	11.8	[56]
Sugar beet industrial filter cake waste	64.1	[57]
Cockleshells (CS)	4.65	This work

The Freundlich model (1906) is a model that applies the data for multilayer and heterogeneous surfaces, the model equation being as follows [58]:

$$q_e = K_F * C_e^{\frac{1}{n}} \quad (12)$$

The linearization of Equation (12) gives the following equation:

$$\log q_e = \log K_F + \frac{1}{n} \log C_e \quad (13)$$

where  $K_f$  (mg/g) is a constant related to the adsorption energy. The values of  $1/n$ ,  $K_f$ , and  $R^2$  were calculated and listed in Table 3.

The Tamkin model is used mainly for the retention of gases on solid surfaces. Therefore, several researchers propose applying this model to the adsorption of aqueous solutions on the surface of bio-adsorbents and assume that the adsorbent molecules are retained on the solid surface energetically, since the model is based on the free energy of sorption as a function of binding energy. The linear form of the model is as follows [58]:

$$q_e = \left( \frac{RT}{b} \right) \ln(A_T C_e) = B_T \ln(A_T C_e) \quad (14)$$

$$q_e = B_T \ln(A_T) + B_T \ln(C_e) \quad (15)$$

where  $q_e$  (mg/g) is the maximum adsorption capacity,  $C_e$  (mg/L) is the adsorbate concentration at equilibrium, and  $A_T$ : Tamkin constant (L/g). The Tamkin model equilibrium constant corresponds to the maximum binding energy  $b_T$  (mg/L), which is related to the heat of sorption  $B_T$  (J/mol). The Tamkin constant represents the variation of energy as a function of binding energy. The relevant coefficients can be calculated from three isotherms, such as  $K_L$ ,  $Q_{max}$ ,  $R_L$ ,  $K_f$ ,  $n$ ,  $A$ ,  $B$ , and  $b$ . The values are listed in Table 3.

### 3.4. Thermodynamic Study

Thermodynamic parameters such as Gibbs energy ( $\Delta G$ ), enthalpy ( $\Delta H$ ), and entropy ( $\Delta S$ ) are important parameters for understanding the adsorption process [59]:

$$\Delta G = -RT \ln K_d \quad (16)$$

$$\ln K_d = \frac{\Delta S}{R} - \frac{\Delta H}{RT} \quad (17)$$

where  $R$  is the constant of perfect gases (8.31 j/mol·K),  $K_d$  represents the thermodynamic equilibrium constant, and  $T$  represents the absolute temperature in ( $K^\circ$ ). Figure 12 shows the variation of  $\ln K_d$  as a function of  $1/T$ . The determined slope and intercept are used to calculate  $\Delta H$  and  $\Delta S$ .

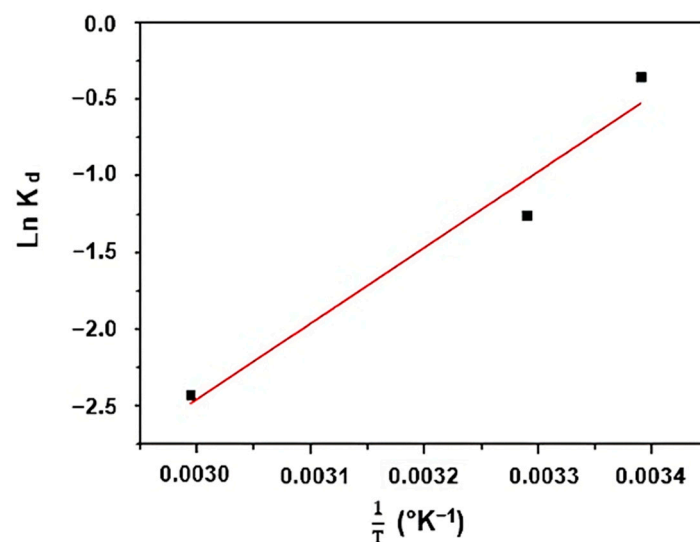


**Figure 12.** Plot of  $\ln(K_d)$  vs.  $1/T$  for removal of DR-81 by CS.

The standard exchange enthalpy was calculated from the Van't Hoff equation (see Table 5), and the negative value  $\Delta H = -41.16$  kJ/mol, which indicates that this is an exothermic adsorption process [60]. The negative value of entropy ( $\Delta S^\circ = -0.144$  kJ/mol· $^\circ K$ ) suggests a decrease in disorder at the solid–liquid interface [61]. The negative Gibbs values ( $\Delta G$  from  $-6.87$  to  $-1.26$  kJ/mol) indicate that the process of biosorption of DR-81 on cockleshells is spontaneous in nature and feasible [62,63]. The decrease in  $\Delta G^\circ$  values with increased temperature indicates highly efficient adsorption at low temperatures [64,65].

**Table 5.** Thermodynamic parameters for biosorption of DR-81 onto cockleshells.

T ( $^\circ K$ )	Parameters			$R^2$
	$\Delta G^\circ$ (kJ/mol)	$\Delta H$ (kJ/mol)	$\Delta S$ (kJ/mol· $^\circ K$ )	
295	-1.32			0.96
304	-2.62	-41.16	-0.144	
334	-6.94			

3.5. Data Analysis by Response Surface Methodology

The optimization of the DR-81 textile dye adsorption process by cockleshells was carried out by performing 15 experiments in a Box–Behnken design. The experimental matrix and prediction values are shown in Table 6, and the model fit and significance were analyzed by ANOVA (Table 7). The model is considered significant when the *p*-values < 5%:

$$Y (R\%) = 58.39 - 14.7888X_1 + 16.7988X_2 - 27.3025X_3 + 1.42625X_1^2 + 1.01125X_2^2 - 13.9912X_3^2 + 4.92750X_1X_2 + 6.065X_1X_3 - 2.41X_2X_3 \quad (18)$$

Table 6. The uncoded Box–Behnken design matrix of experiments for DR-81 removal.

Experiences	Reel Values			Coded Values			Y (R %)	
	X1	X2	X3	C (mg/L)	m (g)	pH	Observed	Predicted
1	−1	−1	0	10	0.3	7	61.77	63.75
2	+1	−1	0	100	0.3	7	21.61	24.31
3	−1	+1	0	10	1.5	7	90.19	87.49
4	+1	+1	0	100	1.5	7	69.74	67.77
5	−1	0	−1	10	0.9	2	93.17	94.00
6	+1	0	−1	100	0.9	2	52.15	52.25
7	−1	0	+1	10	0.9	12	27.33	27.23
8	+1	0	+1	100	0.9	12	10.65	9.82
9	0	−1	−1	55	0.3	2	56.31	53.50
10	0	+1	−1	55	1.5	2	90.05	91.92
11	0	−1	+1	55	0.3	12	5.59	3.72
12	0	+1	+1	55	1.5	12	29.62	32.50
13	0	0	0	55	0.9	7	58.39	58.39
14	0	0	0	55	0.9	7	58.39	58.39
15	0	0	0	55	0.9	7	58.39	58.39

Table 7. ANOVA for the fit of the experimental results to the response surface model.

Factor	DF	Sum of Squares	Mean Square	F-Value	<i>p</i> -Value
Regression	9	10,998.8	1222.09	131.22	0.000
Linear	3	9970.7	3323.55	356.87	0.000
C (mg/L)	1	1749.7	1749.66	187.87	0.000
m (g)	1	2257.6	2257.58	242.41	0.000
pH	1	5963.4	5963.41	640.33	0.000
Square	3	759.7	253.22	27.19	0.002
C (mg/L) * C (mg/L)	1	20.7	7.51	0.81	0.410
m (g) * m (g)	1	16.2	3.78	0.41	0.552
pH * pH	1	722.8	722.79	77.61	0.000
Interaction	3	268.5	89.49	9.61	0.016
C (mg/L) * m (g)	1	97.1	97.12	10.43	0.023
C (mg/L) * pH	1	148.1	148.11	15.90	0.010
m (g) * pH	1	23.2	23.23	2.49	0.175
Residual	5	46.6	9.31		
Lack of fit	3	46.6	15.52	3.77	0.217
Pure error	2	0.0	0.0		
Total	14	11,045.3			

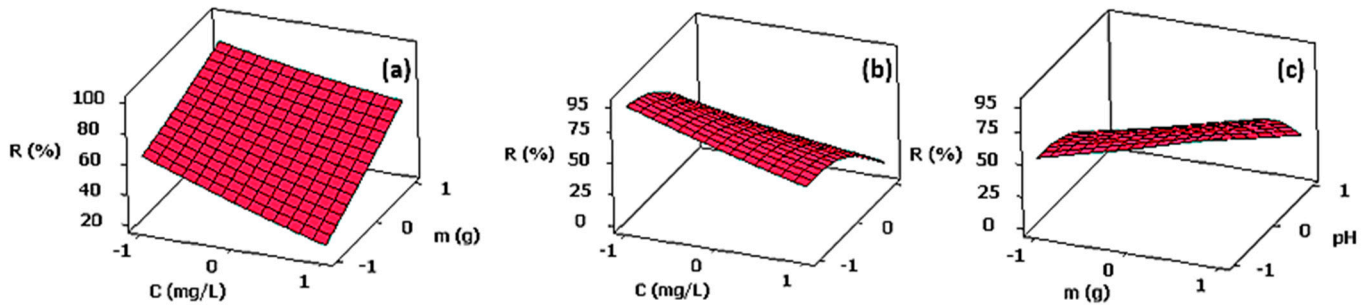
S = 3.05172; R<sup>2</sup> = 99.58%; R<sup>2</sup> (adj) = 98.82%; R<sup>2</sup> (pred) = 93.25%.

Table 6 shows that the individual effects of concentration (X1), mass (X2), and pH (X3) are significant, since the *p*-values < 0. The regression *p*-value of less than 0.001 indicates that the model is favorable for studying the biosorption process of DR-81.

The surface trace was used to develop the potential relationship between the three variables (C, m, and pH). The surface trace in Figure 13a shows that good removal of



DR-81 by CS was achieved at a concentration of 10 mg/L and at a biosorbent dose of 1.5 g. Figure 13b shows that there is maximum dye removal for a concentration of 10 mg/L and a pH of 2. Figure 13c shows that a pH of 2 and a bio-adsorbent dose of 1.5 g give a good DR-81 dye removal efficiency.



**Figure 13.** Three-dimensional (3D) response surface plots for DR-81 removal efficiency by CS: (a) effect of initial concentration/adsorbent dose; (b) effect of initial concentration/pH; (c) effect of adsorbent dose/pH.

Optimization by Minitab@16 software was used to create the graph in Figure 14a, which shows that the maximum yield of the bio-adsorption process was higher than 100% and the desirability  $d = 1$  for the following operating conditions:  $C = 10 \text{ mg/L}$ ;  $m = 1.5 \text{ g}$ ;  $\text{pH} = 2$ . Figure 14b represents the optimal graph of the experimental results applied to the quadratic model, giving the following results:  $C = 10 \text{ mg/L}$ ;  $m = 1 \text{ g}$ ;  $\text{pH} = 2$ . The yield is 96.41%, with a desirability  $d = 0.965$ .

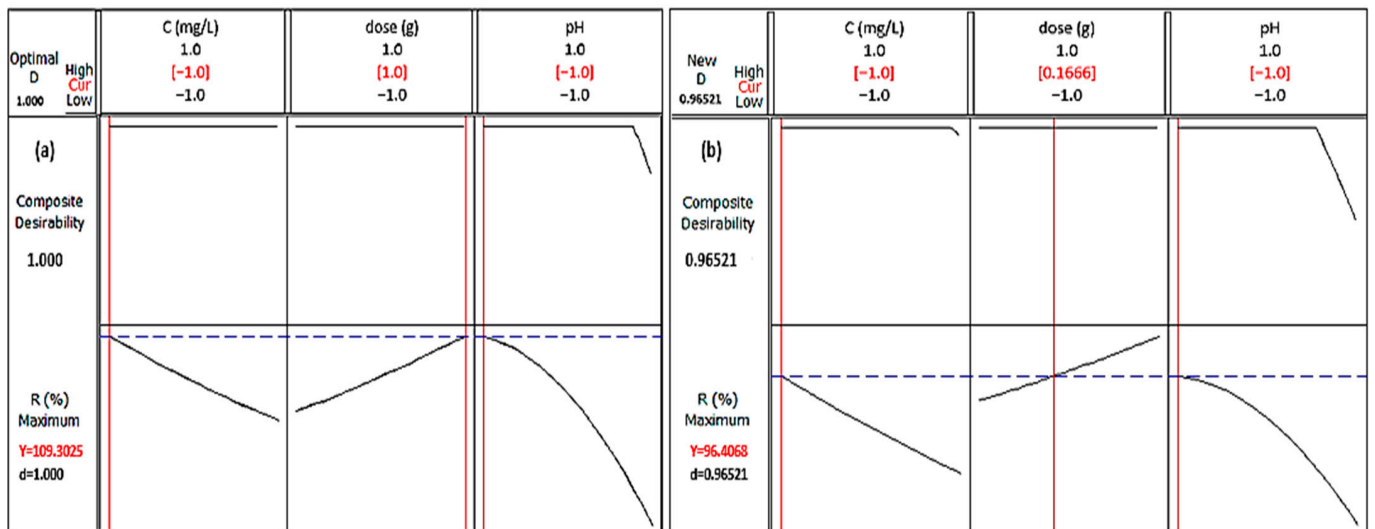


**Figure 14.** Process optimization for DR-81 removal (a) maximum yield of the bio-adsorption process by Minitab (b) optimal yield of the experimental results applied to the quadratic model.

Figure 15 shows that the experimental values ( $R^2 = 99.58\%$ ) are close to the predicted value (93.25%), since the alignment of the scatterplots is very close to the straight line ( $R^2_{adj} = 98.82\%$ ), indicating that the model is relevant, valid, and usable.

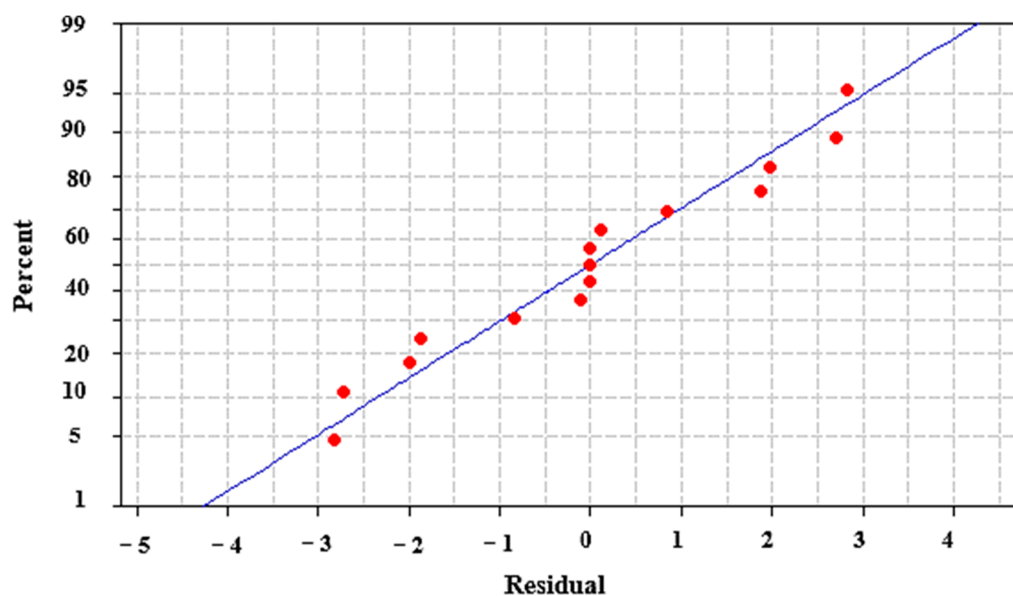


Figure 15. Normal probability plot.

#### 4. Conclusions

The experimental study of the elimination of an anionic dye such as DR-81 from an aqueous solution was carried out by studying the effects of contact time, initial concentration of DR-81, dose of biosorbent, and temperature.

The kinetic study showed that the elimination process of DR-81 follows the pseudo-second-order kinetic model. The isothermal model of Langmuir represents the adsorption process of DR-81, with a correlation coefficient of 0.982. The maximum adsorption capacity is:  $q_{\max} = 4.65$  mg/g at a temperature of 22 °C.

The modeling and optimization of the DR-81 biosorption process by the Box–Behnken scheme gave a very satisfactory yield with a desirability  $d = 1$  under the following conditions:  $C_0 = 10$  mg/L, biosorbent dose = 1.5 g, and pH = 2 at  $T = 22$  °C. The experimental and Box–Behnken results showed convergence between them.

The use of cockleshells for the removal of dyes from anionic textiles is very efficient and cost-effective.

**Author Contributions:** Conceptualization, Z.L., R.B., A.M., A.K., K.D. and A.B.; methodology, Z.L., A.K., A.P. (Antonio Pizzi), A.F.G., A.B. and K.D.; formal analysis, A.K. and A.B.; investigation, Z.L. and K.D.; data curation, Z.L., A.K., A.F.G., A.P. (Antonio Panico) and K.D.; writing—original draft preparation, Z.L., A.M., R.B., A.K., K.D., A.B. and A.P.; writing—review and editing, K.D., R.B., A.P. (Antonio Panico) and A.P. (Antonio Pizzi); supervision, K.D., A.K., Z.L. and A.P. (Antonio Pizzi); project administration, A.K. and K.D. All authors have read and agreed to the published version of the manuscript.

**Funding:** This research received no external funding.

**Institutional Review Board Statement:** Not applicable.

**Informed Consent Statement:** Not applicable.

**Data Availability Statement:** The data that support the findings of this study are available upon request from the corresponding author.

**Acknowledgments:** This work was supported by the University of Constantine 3 (Algeria) and National Polytechnic School of Constantine (Algeria).

**Conflicts of Interest:** The authors declare no conflict of interest.

## References

1. Ahmad, K.; Shah, H.-R.; Ashfaq, M.; Shah, S.S.A.; Hussain, E.; Naseem, H.A.; Parveen, S.; Ayub, A. Effect of Metal Atom in Zeolitic Imidazolate Frameworks (ZIF-8 & 67) for Removal of  $Pb^{2+}$  &  $Hg^{2+}$  from Water. *Food Chem. Toxicol.* **2021**, *149*, 112008. [[CrossRef](#)] [[PubMed](#)]
2. Ismail, M.; Akhtar, K.; Khan, M.I.; Kamal, T.; Khan, M.A.; Asiri, A.M.; Seo, J.; Khan, S.B. Pollution, Toxicity and Carcinogenicity of Organic Dyes and Their Catalytic Bio-Remediation. *Curr. Pharm. Des.* **2019**, *25*, 3645–3663. [[CrossRef](#)] [[PubMed](#)]
3. Haleem, A.; Shafiq, A.; Chen, S.-Q.; Nazar, M. A Comprehensive Review on Adsorption, Photocatalytic and Chemical Degradation of Dyes and Nitro-Compounds over Different Kinds of Porous and Composite Materials. *Molecules* **2023**, *28*, 1081. [[CrossRef](#)] [[PubMed](#)]
4. Zamouche, M.; Tahraoui, H.; Laggoun, Z.; Mechati, S.; Chemchmi, R.; Kanjal, M.I.; Amrane, A.; Hadadi, A.; Mouni, L. Optimization and Prediction of Stability of Emulsified Liquid Membrane (ELM): Artificial Neural Network. *Processes* **2023**, *11*, 364. [[CrossRef](#)]
5. Yagub, M.T.; Sen, T.K.; Afroze, S.; Ang, H.M. Dye and Its Removal from Aqueous Solution by Adsorption: A Review. *Adv. Colloid Interface Sci.* **2014**, *209*, 172–184. [[CrossRef](#)]
6. Alawad, S.M.; Lawal, D.U.; Khalifa, A.E.; Aljundi, I.H.; Antar, M.A.; Baroud, T.N. Analysis of Water Gap Membrane Distillation Process with an Internal Gap Circulation Propeller. *Desalination* **2023**, *551*, 116379. [[CrossRef](#)]
7. Mahmoodi, N.M.; Hayati, B.; Arami, M.; Lan, C. Adsorption of Textile Dyes on Pine Cone from Colored Wastewater: Kinetic, Equilibrium and Thermodynamic Studies. *Desalination* **2011**, *268*, 117–125. [[CrossRef](#)]
8. Amela, K.; Hassen, M.A.; Kerroum, D. Isotherm and Kinetics Study of Biosorption of Cationic Dye onto Banana Peel. *Energy Procedia* **2012**, *19*, 286–295. [[CrossRef](#)]
9. El Mahboub, A.; Ezaier, Y.; Zyade, S.; Mechnou, I. Elaboration and Characterization of Organo-Ghassoul (Moroccan Clay) as an Adsorbent Using Cationic Surfactant for Anionic Dye Adsorption. *Phys. Chem. Res.* **2023**, *11*, 913–928. [[CrossRef](#)]
10. Khalfaoui, A.; Khelifi, M.N.; Khelfaoui, A.; Benalia, A.; Derbal, K.; Gisonni, C.; Crispino, G.; Panico, A. The Adsorptive Removal of Bengal Rose by Artichoke Leaves: Optimization by Full Factorials Design. *Water* **2022**, *14*, 2251. [[CrossRef](#)]
11. Rahman, S.M.A.; Kumar Saha, A.; Ruhi, R.A.; Haque, M.F.; Mohanta, M.K. Decolourization of Textile Azo Dye Direct Red 81 by Bacteria from Textile Industry Effluent. *Int. J. Curr. Microbiol. Appl. Sci.* **2019**, *8*, 1742–1754. [[CrossRef](#)]
12. El-Bendary, M.A.; Ewais, E.A.; Ezzat, S.M.; Al-Zalama, M.A. Process Optimization of the Bio-Decolorization of Textile Dyes by Spore-Bound Laccase of *Bacillus Amyloliquefaciens*. *Microbiology* **2019**, *13*, 23–33.
13. Kebir, M.; Tahraoui, H.; Chabani, M.; Trari, M.; Noureddine, N.; Assadi, A.A.; Amrane, A.; Ben Hamadi, N.; Khezami, L. Water Cleaning by a Continuous Fixed-Bed Column for Cr(VI) Eco-Adsorption with Green Adsorbent-Based Biomass: An Experimental Modeling Study. *Processes* **2023**, *11*, 363. [[CrossRef](#)]
14. Goci, M.C.; Leudjo Taka, A.; Martin, L.; Klink, M.J. Chitosan-Based Polymer Nanocomposites for Environmental Remediation of Mercury Pollution. *Polymers* **2023**, *15*, 482. [[CrossRef](#)] [[PubMed](#)]
15. Tejada-Tovar, C.N.; Rocha-Caicedo, M.M.; Paz-Astudillo, I.C. The Use of Agro-Industrial Residues of Coffee (*Coffea arabica*) for the Removal of Mercury from Water. *J. Water Land Dev.* **2023**, 164–171. [[CrossRef](#)]
16. Mohamad Yusop, M.F.; Tamar Jaya, M.A.; Idris, I.; Abdullah, A.Z.; Ahmad, M.A. Optimization and Mass Transfer Simulation of Remazol Brilliant Blue R Dye Adsorption onto Meranti Wood Based Activated Carbon. *Arab. J. Chem.* **2023**, *16*, 104683. [[CrossRef](#)]
17. Aragaw, T.A.; Alene, A.N. A Comparative Study of Acidic, Basic, and Reactive Dyes Adsorption from Aqueous Solution onto Kaolin Adsorbent: Effect of Operating Parameters, Isotherms, Kinetics, and Thermodynamics. *Emerg. Contam.* **2022**, *8*, 59–74. [[CrossRef](#)]
18. Zambrano-Intriago, L.A.; Daza-López, E.V.; Fernández-Andrade, A.; Luque, R.; Amorim, C.G.; Araújo, A.N.; Rodríguez-Díaz, J.M.; Montenegro, M.C.B.S.M. Application of a Novel Hybrid MIL-53(Al)@rice Husk for the Adsorption of Glyphosate in Water: Characteristics and Mechanism of the Process. *Chemosphere* **2023**, *327*, 138457. [[CrossRef](#)]
19. Maheshwari, U.; Thakur, R.V.; Deshpande, D.; Ghodke, S. Efficiency Evaluation of Orange and Banana Peels for Dye Removal from Synthetic Industrial Effluent. *Mater. Today Proc.* **2023**, *76*, 170–176. [[CrossRef](#)]
20. Sanmuga Priya, E.; Senthamil Selvan, P. Water Hyacinth (*Eichhornia Crassipes*)—An Efficient and Economic Adsorbent for Textile Effluent Treatment—A Review. *Arab. J. Chem.* **2017**, *10*, S3548–S3558. [[CrossRef](#)]
21. Phaenark, C.; Jantrasakul, T.; Paejaroen, P.; Chunchob, S.; Sawangproh, W. Sugarcane Bagasse and Corn Stalk Biomass as a Potential Sorbent for the Removal of Pb(II) and Cd(II) from Aqueous Solutions. *Trends Sci.* **2023**, *20*, 6221. [[CrossRef](#)]
22. Jawad, A.H.; Sauodi, M.; Mastuli, M.S.; Aouda, M.; Radzun, K. Pomegranate Peels Collected from Fresh Juice Shop as a Renewable Precursor for High Surface Area Activated Carbon with Potential Application for Methylene Blue Adsorption. *Desalination Water Treat.* **2018**, *124*, 287–296. [[CrossRef](#)]
23. Tariq, W.; Arslan, C.; Tayyab, N.; Rashid, H.; Nasir, A. Chapter 9—Application of Agro-Based Adsorbent for Removal of Heavy Metals. In *Emerging Techniques for Treatment of Toxic Metals from Wastewater*; Elsevier: Amsterdam, The Netherlands, 2023; pp. 157–182, ISBN 978-0-12-822880-7.
24. Behloul, H.; Ferkous, H.; Bougdah, N.; Djellali, S.; Alam, M.; Djilani, C.; Sedik, A.; Lerari, D.; Jeon, B.-H.; Benguerba, Y. New Insights on the Adsorption of CI-Reactive Red 141 Dye Using Activated Carbon Prepared from the  $ZnCl_2$ -Treated Waste Cotton Fibers: Statistical Physics, DFT, COSMO-RS, and AIM Studies. *J. Mol. Liq.* **2022**, *364*, 119956. [[CrossRef](#)]

25. Nayeem, A.; Mizi, F.; Ali, M.F.; Shariffuddin, J.H. Utilization of Cockle Shell Powder as an Adsorbent to Remove Phosphorus-Containing Wastewater. *Environ. Res.* **2023**, *216*, 114514. [[CrossRef](#)] [[PubMed](#)]
26. Panpho, P.; Vittayakorn, N.; Sumang, R. Synthesis, Scrutiny, and Applications of Bio-Adsorbents from Cockle Shell Waste for the Adsorption of Pb and Cd in Aqueous Solution. *Crystals* **2023**, *13*, 552. [[CrossRef](#)]
27. Khamparia, S.; Jaspal, D. Adsorptive Removal of Direct Red 81 Dye from Aqueous Solution onto Argemone Mexicana. *Sustain. Environ. Res.* **2016**, *26*, 117–123. [[CrossRef](#)]
28. Bohli, T.; Ouederni, A.; Fiol, N.; Villaescusa, I. Evaluation of an Activated Carbon from Olive Stones Used as an Adsorbent for Heavy Metal Removal from Aqueous Phases. *Comptes Rendus Chim.* **2015**, *18*, 88–99. [[CrossRef](#)]
29. Richard, D.; Daouda, A.; Arnaud, M.A.G.; Balike, M. Optimization of Methylene Blue Adsorption onto Activated Carbon from Bos Indicus Gudali Bones Using a Box Behnken Experimental Design. *Am. J. Chem.* **2022**, *12*, 1–9. [[CrossRef](#)]
30. Zamouche, M.; Habib, A.; Saaidia, K.; Bencheikh Lehocine, M. Batch Mode for Adsorption of Crystal Violet by Cedar Cone Forest Waste. *SN Appl. Sci.* **2020**, *2*, 198. [[CrossRef](#)]
31. Kamba, A.S.; Ismail, M.; Ibrahim, T.A.T.; Zakaria, Z.A.B. Synthesis and Characterisation of Calcium Carbonate Aragonite Nanocrystals from Cockle Shell Powder (Anadara Granosa). *J. Nanomater.* **2013**, *2013*, 5. [[CrossRef](#)]
32. Hussein, A.I.; Ab-Ghani, Z.; Che Mat, A.N.; Ab Ghani, N.A.; Husein, A.; Ab Rahman, I. Synthesis and Characterization of Spherical Calcium Carbonate Nanoparticles Derived from Cockle Shells. *Appl. Sci.* **2020**, *10*, 7170. [[CrossRef](#)]
33. Mohd Abd Ghafar, S.L.; Hussein, M.Z.; Abu Bakar Zakaria, Z. Synthesis and Characterization of Cockle Shell-Based Calcium Carbonate Aragonite Polymorph Nanoparticles with Surface Functionalization. *J. Nanoparticles* **2017**, *2017*, 20–22. [[CrossRef](#)]
34. Aldemir, A.; Turan, A.; Kul, A.R.; Koyuncu, H. Comprehensive Investigation of Basic Red 46 Removal by Pinecone Adsorbent: Experimental, Isotherm, Kinetic and Thermodynamic Studies. *Int. J. Environ. Sci. Technol.* **2023**, *20*, 2601–2622. [[CrossRef](#)]
35. Islam, K.N.; Zuki, A.B.Z.; Ali, M.E.; Bin Hussein, M.Z.; Noordin, M.M.; Loqman, M.Y.; Wahid, H.; Hakim, M.A.; Abd Hamid, S.B. Facile Synthesis of Calcium Carbonate Nanoparticles from Cockle Shells. *J. Nanomater.* **2012**, *2012*, 534010. [[CrossRef](#)]
36. Mukhtar, A.; Mellon, N.; Saqib, S.; Lee, S.-P.; Bustam, M.A. Extension of BET Theory to CO<sub>2</sub> Adsorption Isotherms for Ultra-Microporosity of Covalent Organic Polymers. *SN Appl. Sci.* **2020**, *2*, 1232. [[CrossRef](#)]
37. Sy Mohamad, S.F.; Mohamad, S.; Jemaat, Z. Study of Calcination Condition on Decomposition of Calcium Carbonate in Waste Cockle Shell to Calcium Oxide Using Thermal Gravimetric Analysis. *J. Eng. Appl. Sci.* **2016**, *11*, 9917–9921.
38. Ridzwan, N.F.A.A.; Aziz, N.A.; Akbar, N.A.; Ghani, Z.A.; Hamzah, N.; Mohd Zin, N.S. Removal of Mn and Cu Ions in Synthetic Wastewater Using Dried Cockle Shell. *Environ. Ecol. Res.* **2022**, *10*, 31–43. [[CrossRef](#)]
39. Aronson, J.M.; Machlis, L. The Chemical Composition of the Hyphal Walls of the Fungus *Allomyces*. *Am. J. Bot.* **1959**, *46*, 292–300. [[CrossRef](#)]
40. Nozari, M. Removal of Direct Red 81 Dye from Aqueous Solution Using Neutral Soil Containing Copper. *Desalination Water Treat.* **2018**, *86*, 213–220. [[CrossRef](#)]
41. Msaadi, R.; Sassi, W.; Hihn, J.-Y.; Ammar, S.; Chehimi, M.M. Valorization of Pomegranate Peel Balls as Bioadsorbents of Methylene Blue in Aqueous Media. *Emergent Mater.* **2022**, *5*, 381–390. [[CrossRef](#)]
42. Zamouche, M.; Chermat, M.; Kermiche, Z.; Tahraoui, H.; Kebir, M.; Bollinger, J.-C.; Amrane, A.; Mouni, L. Predictive Model Based on K-Nearest Neighbor Coupled with the Gray Wolf Optimizer Algorithm (KNN\_GWO) for Estimating the Amount of Phenol Adsorption on Powdered Activated Carbon. *Water* **2023**, *15*, 493. [[CrossRef](#)]
43. Ruscasso, F.; Bezus, B.; Garmendia, G.; Vero, S.; Curutchet, G.; Cavello, I.; Cavalitto, S. *Debaryomyces Hansenii* F39A as Biosorbent for Textile Dye Removal. *Rev. Argent. Microbiol.* **2021**, *53*, 257–265. [[CrossRef](#)] [[PubMed](#)]
44. Bellir, K.; Bouziane, I.S.; Boutamine, Z.; Lehocine, M.B.; Meniai, A.-H. Sorption Study of a Basic Dye “Gentian Violet” from Aqueous Solutions Using Activated Bentonite. *Energy Procedia* **2012**, *18*, 924–933. [[CrossRef](#)]
45. Berrazoum, A.; Marouf, R.; Ouadjenia, F.; Schott, J. Bioadsorption of a Reactive Dye from Aqueous Solution by Municipal Solid Waste. *Biotechnol. Rep.* **2015**, *7*, 44–50. [[CrossRef](#)] [[PubMed](#)]
46. Jawad, A.H.; Mohd Firdaus, N.N.; Hum, M.; Farhan, A.; Mastuli, M.S.; Farhan, A. Biosorption of Methylene Blue Dye by Rice (*Oryza sativa* L.) Straw: Adsorption and Mechanism Study. *Desalin Water Treat.* **2020**, *190*, 322–330. [[CrossRef](#)]
47. Faisal, A.A.H.; Ibreesam, M.M.; Al-Ansari, N.; Naji, L.A.; Naushad, M.; Ahamad, T. COMSOL Multiphysics 3.5a Package for Simulating the Cadmium Transport in the Sand Bed-Bentonite Low Permeable Barrier. *J. King Saud Univ.-Sci.* **2020**, *32*, 1944–1952. [[CrossRef](#)]
48. Cheikh, S.; Imessaoudene, A.; Bollinger, J.-C.; Hadadi, A.; Manseri, A.; Bouzaza, A.; Assadi, A.; Amrane, A.; Zamouche, M.; El Jery, A.; et al. Complete Elimination of the Ciprofloxacin Antibiotic from Water by the Combination of Adsorption-Photocatalysis Process Using Natural Hydroxyapatite and TiO<sub>2</sub>. *Catalysts* **2023**, *13*, 336. [[CrossRef](#)]
49. Bajaber, M.A.; Anjum, M.N.; Ibrahim, M.; Farooq, T.; Ahmad, M.N.; Abideen, Z.u. Synthesis and Characterization of Hydroxyethyl Cellulose Grafted with Copolymer of Polyaniline and Polypyrrole Biocomposite for Adsorption of Dyes. *Molecules* **2022**, *27*, 8238. [[CrossRef](#)]
50. Hossein, M.A.; Behzad, H. Removal of Reactive Red 120 and Direct Red 81 Dyes from Aqueous Solutions by Pumice. *Res. J. Chem. Environ.* **2012**, *16*, 62–68.
51. Ali, I.; Dahiya, S.; Khan, T. Removal of Direct Red 81 Dye from Aqueous Solution by Native and Citric Acid Modified Bamboo Sawdust-Kinetic Study and Equilibrium Isotherm Analyses. *Gazi Univ. J. Sci.* **2012**, *25*, 59–87.

52. Momen, H.M.; Kodabande, A.; Bozorgmehr, M.R.; Ardalan, T.; Ardalan, P. Kinetic and Thermodynamic Studies on Biosorption of Direct Red 81 from Aqueous Solutions by Chamomilla Plant. *J. Chem. Health Risks* **2012**, *2*, 37–43.
53. Sharma, N.; Tiwari, D.P.; Singh, S.K. Efficiency of Chemically Treated Potato Peel and Neem Bark For Sorption of Direct Red-81 Dye from Aqueous Solution. *Rasayan J. Chem.* **2014**, *7*, 399–409.
54. Momen, H.M.; Ardalan, P.; Vafaie, A. Equilibrium and Kinetic Studies of Direct Red Biosorption Onto Modified Silk Maze as an Economical Biosorbent. *J. Chem. Health Risks* **2014**, *4*, 63–73.
55. Dehghani, M.; Nozari, M.; Fakhraei Fard, A.; Ansari Shiri, M.; Shamsedini, N. Direct Red 81 Adsorption on Iron Filings from Aqueous Solutions; Kinetic and Isotherm Studies. *Environ. Technol.* **2019**, *40*, 1705–1713. [[CrossRef](#)] [[PubMed](#)]
56. Azizi, A.; Moniri, E.; Hassani, A.H.; Ahmad Panahi, H. Reusability, Optimization, and Adsorption Studies of Modified Graphene Oxide in the Removal of Direct Red 81 Using Response Surface Methodology. *Adv. Environ. Technol.* **2020**, *6*, 175–185. [[CrossRef](#)]
57. Aly, A.; Abd El-Wahab, M.; Hassan, S.; Abd El-Ghany, I.; Farrag, A. Utilization of Sugar Beet Industrial Filter Cake Waste for Removal of Direct Red 81 from Aqueous Solution. *Egypt. Sugar J.* **2021**, *16*, 77–96. [[CrossRef](#)]
58. Jamoussi, B.; Chakroun, R.; Jablaoui, C.; Rhazi, L. Efficiency of Acacia Gummifera Powder as Biosorbent for Simultaneous Decontamination of Water Polluted with Metals. *Arab. J. Chem.* **2020**, *13*, 7459–7481. [[CrossRef](#)]
59. Da Costa, T.B.; da Silva, M.G.C.; Vieira, M.G.A. Crosslinked Alginate/Sericin Particles for Bioadsorption of Ytterbium: Equilibrium, Thermodynamic and Regeneration Studies. *Int. J. Biol. Macromol.* **2020**, *165*, 1911–1923. [[CrossRef](#)]
60. Ammendola, P.; Raganati, F.; Chirone, R. CO<sub>2</sub> Adsorption on a Fine Activated Carbon in a Sound Assisted Fluidized Bed: Thermodynamics and Kinetics. *Chem. Eng. J.* **2017**, *322*, 302–313. [[CrossRef](#)]
61. Uddin, M.K.; Nasar, A. Walnut Shell Powder as a Low-Cost Adsorbent for Methylene Blue Dye: Isotherm, Kinetics, Thermodynamic, Desorption and Response Surface Methodology Examinations. *Sci. Rep.* **2020**, *10*, 7983. [[CrossRef](#)]
62. Kocaman, S. Removal of Methylene Blue Dye from Aqueous Solutions by Adsorption on Levulinic Acid-Modified Natural Shells. *Int. J. Phytoremed.* **2020**, *22*, 885–895. [[CrossRef](#)] [[PubMed](#)]
63. Bouhedda, M.; Lefnaoui, S.; Rebouh, S.; Yahoum, M.M. Predictive Model Based on Adaptive Neuro-Fuzzy Inference System for Estimation of Cephalexin Adsorption on the Octenyl Succinic Anhydride Starch. *Chemom. Intell. Lab. Syst.* **2019**, *193*, 103843. [[CrossRef](#)]
64. Bouchelkia, N.; Tahraoui, H.; Amrane, A.; Belkacemi, H.; Bollinger, J.-C.; Bouzaza, A.; Zoukel, A.; Zhang, J.; Mouni, L. Jujube Stones Based Highly Efficient Activated Carbon for Methylene Blue Adsorption: Kinetics and Isotherms Modeling, Thermodynamics and Mechanism Study, Optimization via Response Surface Methodology and Machine Learning Approaches. *Process Saf. Environ. Prot.* **2023**, *170*, 513–535. [[CrossRef](#)]
65. Methylene Blue Adsorption from Aqueous Solution by Low Cost Vine-Wood Biomass. Available online: <https://www.researchsquare.com> (accessed on 27 August 2023).

**Disclaimer/Publisher’s Note:** The statements, opinions and data contained in all publications are solely those of the individual author(s) and contributor(s) and not of MDPI and/or the editor(s). MDPI and/or the editor(s) disclaim responsibility for any injury to people or property resulting from any ideas, methods, instructions or products referred to in the content.